Exploring carbon source related localization and phosphorylation in the Snf1/Mig1 network using population and single cell-based approaches

microbial cell

Research Article

www.microbialcell.com

Exploring carbon source related localization and phosphorylation in the Snf1/Mig1 network using population and single cell-based approaches

Svenja Braam[1], Farida Tripodi[2,*], Linnea Österberg[1,3], Sebastian Persson[1], Niek Welkenhuysen[1,3], Paola Coccetti[2] and Marija Cvijovic[1,*]

[1]Department of Mathematical Sciences, Chalmers University of Technology, University of Gothenburg, Sweden. [2]Department of Biotechnology and Biosciences, University of Milano Bicocca, Italy. [3]Department of Biology and Biological Engineering, Chalmers University of Technology, Sweden

*Corresponding Authors:
Farida Tripodi, Department of Biotechnology and BiosciencesUniversity of Milano-Bicocca, Piazza della Scienza 2, 20126 Milano, Italy; phone: +39 264483513; E-mail: farida.tripodi1@unimib.it
Marija Cvijovic, Department of Mathematical Sciences, Chalmers University of Technology and University of Gothenburg, SE-412 96 Gothenburg, Sweden; phone: +46 317725321; E-mail: marija.cvijovic@chalmers.se

ABSTRACT The AMPK/SNF1 pathway governs energy balance in eukaryotic cells, notably influencing glucose de-repression. In *S. cerevisiae*, Snf1 is phosphorylated and hence activated upon glucose depletion. This activation is required but is not sufficient for mediating glucose de-repression, indicating further glucose-dependent regulation mechanisms. Employing fluorescence recovery after photobleaching (FRAP) in conjunction with non-linear mixed effects modelling, we explore the spatial dynamics of Snf1 as well as the relationship between Snf1 phosphorylation and its target Mig1 controlled by hexose sugars. Our results suggest that inactivation of Snf1 modulates Mig1 localization and that the kinetic of Snf1 localization to the nucleus is modulated by the presence of non-fermentable carbon sources. Our data offer insight into the true complexity of regulation of this central signaling pathway in orchestrating cellular responses to fluctuating environmental cues. These insights not only expand our understanding of glucose homeostasis but also pave the way for further studies evaluating the importance of Snf1 localization in relation to its phosphorylation state and regulation of downstream targets.

doi: 10.15698/mic2024.05.822
Received originally: 14. 06. 2023;
in revised form: 05. 03. 2024,
Accepted: 12. 03. 2024
Published: 16.05.2024

Keywords: yeast, nutrient signaling, Snf1/Mig1 network, nuclear localization, fluorescence recovery after photobleaching, nonlinear mixed effect model

Abbreviations:
FRAP - fluorescence recovery after photobleaching,
NLME - nonlinear mixed-effects.

Introduction

Protein kinases within the Snf1/AMPK family are highly conserved master regulators of energy homeostasis in eukaryotic cells [1, 2]. They mediate signaling of energy demand, a process central to ensure continuous cell growth and cell development, one of the most important aspects of a cell's lifecycle.

In the yeast *Saccharomyces cerevisiae*, Snf1 is involved in adaptation to glucose limitation when the use of alternative carbon sources is needed to achieve growth and proliferation [3–5]. The Snf1 signaling pathway also affects a broad spectrum of downstream functions, such as lipid biogenesis and gluconeogenesis to balance energy demand and supply [6, 7]. In addition to its role in energy homeostasis, Snf1 participates in several stress signaling pathways, indicating a more extensive involvement [4, 8].

Snf1 is the catalytic subunit of the heterotrimeric complex that we will refer to as SNF1 throughout this paper. This complex consists of the regulatory γ-subunit Snf4 and one of three alternative β-subunits, Gal83, Sip1 or Sip2 [9, 10]. The β-subunits control the location of the SNF1 complex within the cell [11], and assembly in a complex with the γ-subunit and any of the β-subunits is necessary for stable Snf1 kinase activity [9, 10, 12].

Previous studies have indicated that localization of the various β-subunits to cell compartments differs depending on carbon source [11, 13]. Shifting the carbon source in the medium from high glucose content to ethanol results in localization of SNF1 to the nucleus [11].

One important mechanism that involves SNF1 is glucose de-repression, which describes the cell's preference to utilize glucose over alternative carbon sources and is mediated by the phosphorylation and dephosphorylation of Snf1. Continuous phosphorylation of Snf1 via the three upstream kinases Sak1, Tos3 and Elm1 activates the expression of genes that are necessary for utilizing alternative carbon sources [14–17].

Dephosphorylation of Snf1 takes place rapidly by the PP1 phosphatases Reg1/2-Glc7, Sit4 or Ptc2 as soon as a preferred sugar such as the hexose sugars glucose, fructose or mannose becomes available [18–21].

Active Snf1 phosphorylates several downstream target proteins, with the transcriptional repressor Mig1 being the most prominent [22, 23]. Unphosphorylated Mig1 locates to the nucleus and mediates the repression of genes required for the utilization of alternative carbon sources [24, 25]. Phosphorylation of Mig1 by Snf1 promotes its exit from the nucleus via the exportin Msn5 [23, 26]. This results in the initiation of glucose de-repression and allows the expression of genes, such as *SUC2* and *HXK1*, which are required for the use of alternative carbon sources [23, 27–29].

Mig1 localization in response to various concentrations of hexoses has been studied before and is established as a measurement for the SNF1 pathway activity [30–33].

However, overexpression of the upstream protein kinase Sak1 or addition of sodium and lithium ions leads to activation of Snf1, but not to glucose de-repression [14, 34]. This leads to the conclusion that SNF1 activation is required but is not sufficient for mediating glucose de-repression and that a second glucose-regulated step governs the Snf1/Mig1 pathway activity [14]. Understanding this aspect is critical because Mig1 is a common measure of SNF1 activity, and both Snf1 and Mig1 play vital roles in utilizing carbon sources.

A proposed model by Vega, Riera, Fernández-Cid, Herrero and Moreno [35], suggests that the Gal83 associated isoform of SNF1 has a structural role in the repression complex of *SUC2*, a gene co-regulated by Mig1 and Mig2. However, the importance of the SNF1 localization for glucose repression remains unclear.

To better understand the localization of Snf1 and its regulation in glucose de-repression, we utilize time-lapse fluorescence microscopy, fluorescence recovery after photobleaching (FRAP) and phosphorylation assays to study the nuclear-cytoplasmic shuttling of Snf1 and Mig1 in response to external carbon sources in various concentrations.

Results

The kinetics of Snf1 nucleocytoplasmic shuttling are driven by carbon source availability

To understand how Snf1 mechanistically mediates glucose de-repression, we employed FRAP. Exponentially grown yeast cells expressing GFP-tagged Snf1 were exposed to YNB supplemented with either 2% glucose (sustaining a fermentative metabolism), 0.05% glucose or 2% glycerol (two conditions in which metabolism is mainly respirative) for at least 1 h before the onset of measurements. Fluorescently tagged Snf1 in the nucleus was bleached, and the subsequent recovery of fluorescence in the nucleus was observed. The obtained data were analyzed by fitting a single exponential model using a nonlinear mixed-effects (NLME) framework (SI data files 2-4 as well as methods section for details, data available via https://github.com/cvijoviclab/Snf1-localization) [36]. The diagnostic plots in Figure 1 show that the model has good predictive power for all conditions tested, although values at the later time points might be underestimated, as can be seen by the outliers in the observed data in comparison to the prediction intervals. The good fit is indicated by the weighted residuals clustering randomly around the x-axis (Figure 1, right panel), and when simulated the fitted model can reproduce the observed data (for detailed plot of observed FRAP curves and predicted values see supplementary information 2-4). Cell size and nucleus size measurements in the cells tested showed that the fraction of the bleached nucleus was unaffected by the conditions applied, indicated by a non-significant Kruskal Wallis test (cell area p = 0.72, nucleus area p = 0.13) and spot tests indicated that Snf1-GFP is functional (Figures S3-4).

The kinetic coefficient (τ) for Snf1-GFP when cells were exposed to 2% glycerol indicates a faster nuclear-cytoplasmic shuttling in comparison to the cells exposed to 2% or 0.05% glucose (Table 1). Activating kinases are typically contained in the cytoplasm and Snf1 nuclear localization is dependent on both, its phosphorylation and on the interaction with Gal83 [11]. Faster recovery for cells exposed to glycerol indicates a mechanism that is independent on glucose concentration but rather on the presence of a fermentable carbon source. The parameters furthermore indicated a large immobile fraction. This could hint towards a large entity of bound Snf1-GFP, for example to the β-subunit Gal83.

To elucidate the steady-state accumulation of Snf1-GFP in the nucleus under these conditions, we compared the fraction of the total Snf1-GFP intensity in the nucleus by employing confocal microscopy. Snf1 steady-state nuclear fractions were comparable under high (2%) and low (0.05%) glucose concentrations (Figure 2A). A non-significant mean fold change of 1.06 (p-value = 0.5479), indicates that under steady-state conditions Snf1 localization was not modulated by glucose concentration.

Together with results from the FRAP measurements, this could suggest that Snf1 nuclear localization is not strongly influenced by changes in concentration of glucose and that the relative difference in glucose concentration has a smaller effect than the type of carbon source itself.

Snf1 phosphorylation status correlates with Mig1 localization upon carbon source upshift

The data from FRAP experiments indicated that Snf1 localization and nucleo-cytoplasmic shuttling parameters depend on the type of carbon source rather than on concentration. We set out to find if this relationship was also present in the short-term phosphorylation pattern of Snf1 in different fermentable sugars at various concentrations. To evaluate the activation state of Snf1 during the shift-up, cells were grown in YNB containing ethanol until mid-exponential phase. Then the fermentable carbon source (glucose, fructose or mannose) at the indicated concentrations was added to the culture. Samples were taken after 5 minutes to measure the pT210-Snf1 level (pSnf1) (Figure 2B and C, Figure S2). When the fermentable carbon source was added to the cells, a reduction of Snf1 phosphorylation was observed, with a magnitude proportional to the concentration added. Glucose was the carbon source which reduced phosphorylation of Snf1 more strongly since it was reduced to 20% already at a concentration of 0.005% and reached maximal reduction at 1% concentration. Fructose and mannose present similarly, with an inhibition of 50% at 0.005%, and a maximal inhibition at 0.5% concentration (Figure 3A).

With the same approach, the initial spatial Mig1 response towards different carbon sources was characterized through fluorescent time-lapse microscopy. Mig1 localization to the

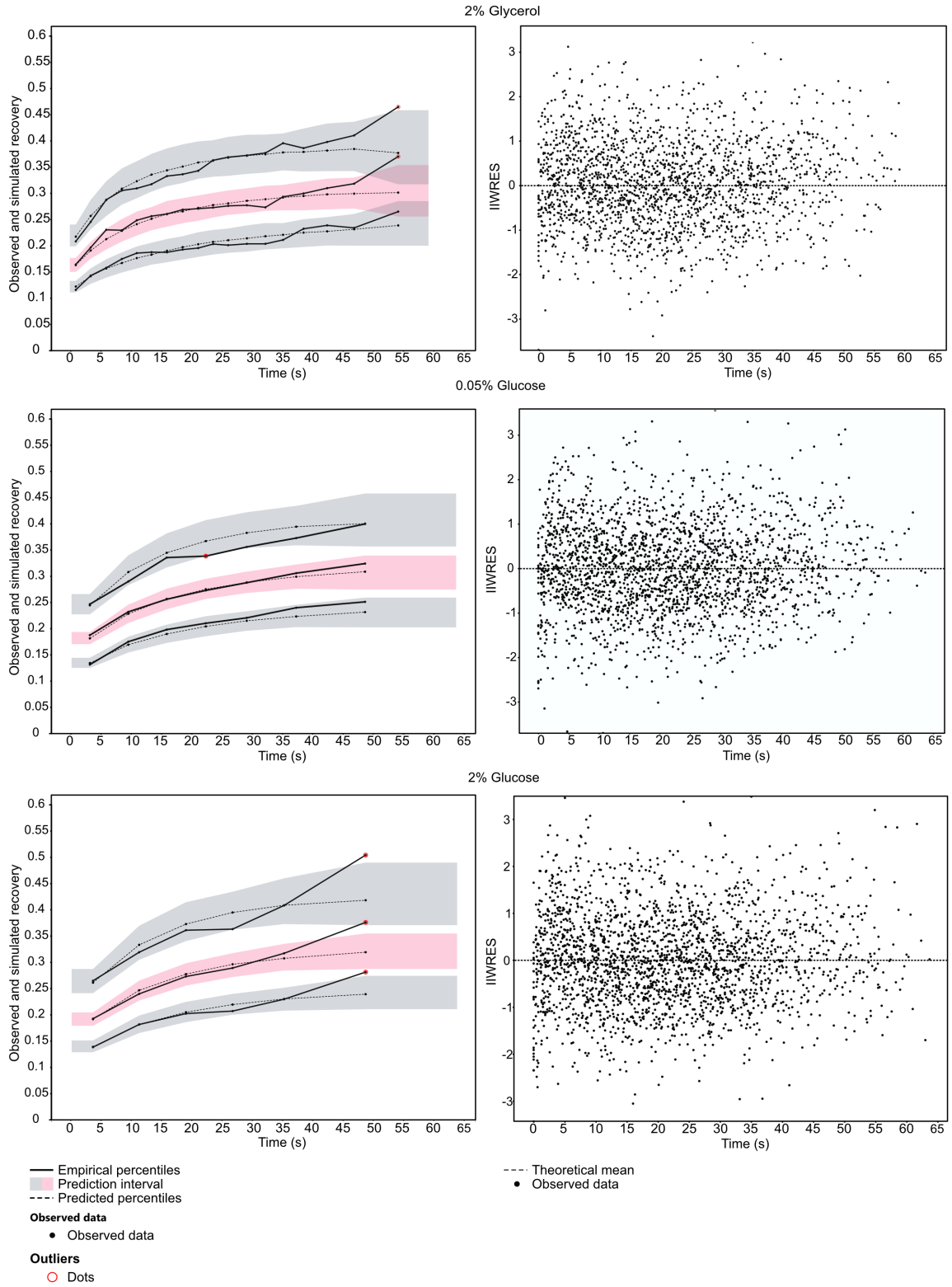

FIGURE 1 ● **Diagnosticplots of the NLME model used to predict population parameters.** Left panel: visual predictive check to determine predictive power of the model. Datapoints were binned using least squares criteria and smoothed using linear interpolation. Solid line determines the observed data in the 10^{th},50^{th} and 90^{th} percentile. Gray/red areas are the prediction intervals for the respective percentile in which 90% of the simulated data lie, determined by 400 Monte Carlo simulations. Right panel: Scatterplots of individual residuals. Dots represent the individual weighted residuals over time represented by conditional mode of the distribution of residuals.

TABLE 1 ● FRAP population parameters for Snf1 separated by the fixed effects (A, τ, I_0) and standard deviation of random effects (ω_{A1}, ω_τ , ω_{I0}), as well as parameters derived from the fixed effects.

	2% glucose		0.05% glucose		2% glycerol	
	Y_p	S.E	Y_p	S.E	Y_p	S.E
A	**0.172**	0.011	**0.168**	0.0103	**0.164**	0.00994
τ	**0.0666**	0.0074	**0.0638**	0.00839	**0.0812**	0.0134
I_0	**0.156**	0.00607	**0.152**	0.0054	**0.152**	0.00615
ω_A	**0.302**	0.0474	**0.279**	0.0466	**0.273**	0.0481
ω_τ	**0.491**	0.0827	**0.566**	0.100	**0.744**	0.123
ω_{I0}	**0.184**	0.0286	**0.160**	0.026	**0.183**	0.0312
Number of cells total	**25**	-	**24**	-	**21**	-
Half-max (s)	**10.407**	-	**10.864**	-	**9.001**	-
Mobile fraction	**0.016**	-	**0.016**	-	**0.012**	-
Immobile fraction	**0. 984**	-	**0.984**	-	**0.988**	-

Representations of the kinetic constant (τ) and mobility (A), the degree of bleaching (I_0) as well as half-max time as representation of recovery rate and calculated mobile fraction representing proteins contributing to recovery and immobile fraction (for details see Method section). Data derived from cells pooled in three independent experiments.

nucleus was observed at 0.005% glucose, while in upshift to mannose and fructose, Mig1 nuclear localization was only observed at concentrations above 0.05% (**Figure 3A** and **Figure 3B** for further exemplary images, Figure S1). These results suggest that the Mig1 nuclear import is more sensitive to glucose than to mannose and fructose, similarly, observed for Snf1 phosphorylation.

In order to better investigate the Snf1-Mig1 pathway, expression of two glucose repressed genes (i.e. *SUC2* and *HXK1*) was analyzed by qPCR. Cells were grown in ethanol-containing YNB medium until mid-exponential phase. Cells were either left in ethanol, or glucose was added to the cultures at 0.05% or 4% final concentration. Samples were taken after 15 and 30 minutes to measure *SUC2* and *HXK1* expression (**Figure 4**). When the fermentable carbon source was added, the expression of both *SUC2* and *HXK1* was strongly reduced, similarly in the presence of low (0.05%) and high (4%) glucose concentration. This suggests that although glucose repression can be seen, expression of glucose repressed genes is not a sensitive readout to evaluate the dose-dependent Snf1 response to carbon sources. This could likely be the result of both transcriptional repression and rapid mRNA degradation that takes place upon glucose addition [37]. The glucose concentration independent recovery time during FRAP further enforces this result by indicating that glucose concentration in the short term does not influence the nuclear import of Snf1 while it does influence the nuclear accumulation of Mig1.

Discussion

In this work we set out to explore the relationship between the subcellular localization and regulation of kinases in the context of carbon source signaling. We show that Snf1 responds to glucose with a decreased recovery rate during FRAP already at low glucose concentrations and that nuanced phosphorylation of Snf1 in response to various concentrations of hexose sugars corresponds with Mig1 localization to the nucleus.

We studied the kinetics of Snf1 nucleocytoplasmic shuttling by employing a FRAP method. Using NLME regression, we were able to determine recovery rates as well as showing that most of the fraction of bleached protein was immobile. Snf1 is part of the pathway wherein the transcriptional repressor Mig1 is responsible for glucose repression. While this pathway has been reported to be activated at higher glucose concentrations [38–40], it has also been shown that gluconeogenic enzymes are tightly repressed even by small amounts of glucose via mechanisms such as mRNA degradation as a short-term reaction to changes in carbon source availability [37, 39]. We furthermore observe the steady-state spatial distribution of Snf1 after exposing yeast cells to various concentrations of glucose and glycerol. The localization of Snf1 in the nucleus is significantly changing when comparing any of the nuclear-cytosolic ratios obtained from glucose-exposed cells to glycerol-exposed cells.

It is not possible to exclude whether residual glucose in the medium of cells exposed to low glucose in our FRAP experiment was present, however, it could indicate that nuclear cytosolic shuttling might be reduced even with small amounts of glucose present in the medium. The observed steady-state nuclear cytoplasmic ratio could be a further hint in this direction. It furthermore cannot be excluded that the reason for the reduced nucleocytoplasmic shuttling could lie in halted translation due to a stress response as reaction to the strong reduction of glucose in the medium in our experimental setting.

Previous studies suggest however, that the levels and the phosphorylation status of Snf1 are reciprocally regulated, as hyperphosphorylation has been observed when the level of Snf1 is lower than normal [41]. Snf1 has been shown to be transiently phosphorylated after a shift to lower glucose indicating that Snf1 could also be involved in mediating cellular changes in response to concentrations of glucose, which affects the level of Snf1 phosphorylation and then its nuclear localization [30]. Phosphorylation of Snf1 already at low concentrations of glucose after a switch from a non-fermentable carbon source in our study might further confirm the tight regulation of glucose repressed genes in the presence of even low amounts of glucose.

Gal83, the β-subunit responsible for Snf1 localization to the nucleus, has been shown to be detected in the nucleus after a shift to low glucose [11]. One interpretation could entail

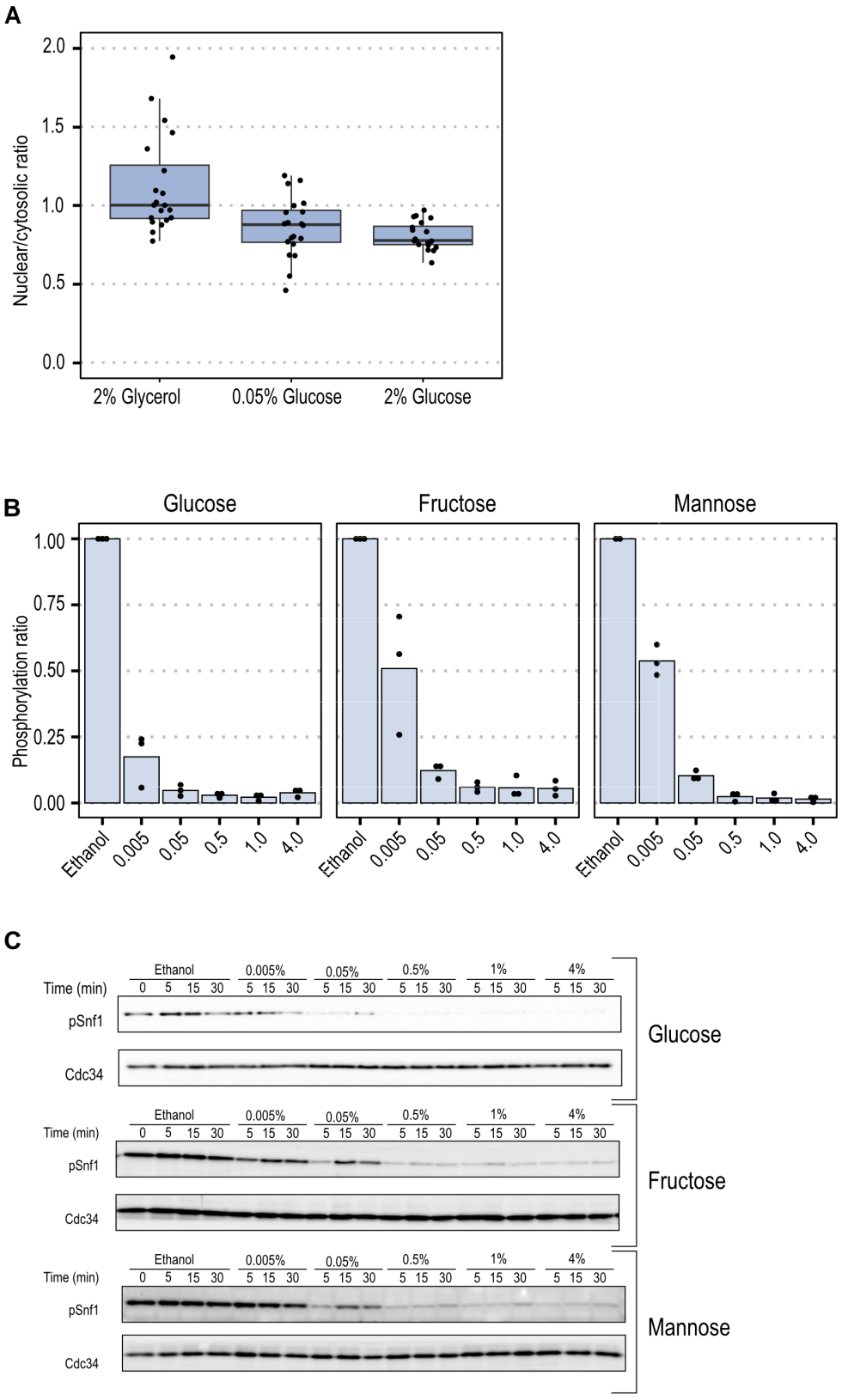

FIGURE 2 ● **Snf1localization and Snf1 phosphorylation.** (A) The nuclear-cytosolic ratio of Snf1-GFP was calculated by dividing the mean of the fluorescence of Snf1-GFP in the nucleus with the mean of the fluorescence in the cytosol. Horizontal lines indicate the mean, the boxplot has as lower and upper hinge respectively the 25^{th} and 75^{th} percentile and the whiskers denote the 95% confidence interval. Dots denote individual cells. (B) Mean of relative Snf1 phosphorylation by western blot quantification 5 minutes after upshift from ethanol to glucose, fructose or mannose, dots represent biological replicates. (C) Exemplary images of the western blot showing phosphorylated Snf1.

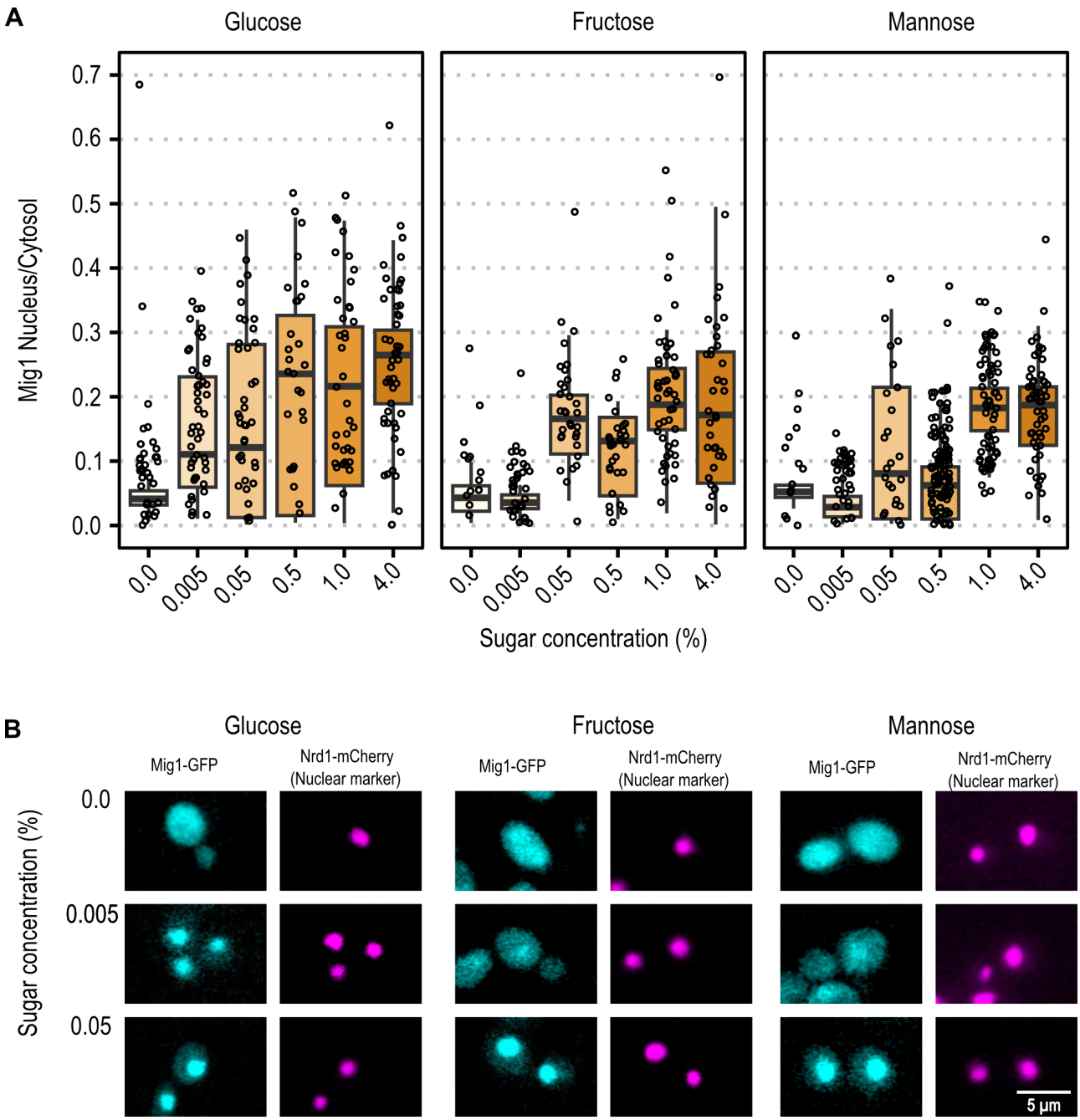

FiGURE 3 ● **Mig1nuclear localization after upshift.** (A) Mig1 nuclear localization ratio in cells 5 minutes after the shift from ethanol to the indicated concentration of glucose, fructose, or mannose. Horizontal lines indicate the mean, the boxplot has as lower and upper hinge respectively the 25^{th} and 75^{th} percentile and the whiskers denote the 95% confidence interval. Dots denote individual cells. (B) Microscopic images of single cells, representative for the tested cells in panel B, 5 minutes after shift from ethanol to the indicated conditions. Mig1-GFP is displayed in cyan and Nrd1-mCherry in magenta. Brightness and contrast have been adjusted for better visibility.

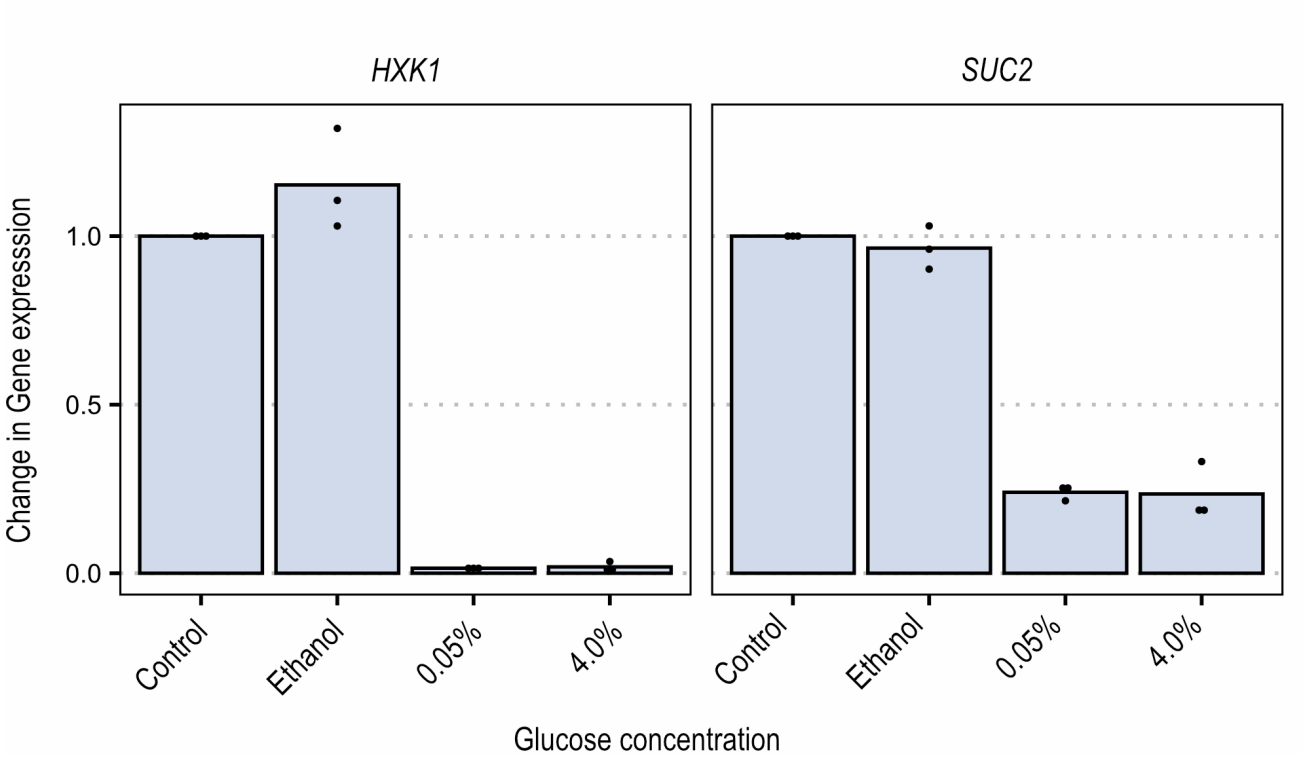

FIGURE 4 ● **Expression of *HXK1* and *SUC2* measured via qPCR, 15 minutes after shift to glucose.** Data are shown as ratio change of gene expression. Control: baseline expression of cultures grown in ethanol at start of measurements. Dots represent biological replicates.

that cells with a large fraction of the Snf1 pool bound to other processes need a higher activity of the nucleocytoplasmic shuttling to serve the same function. Under exposure to glycerol, this could indicate that a lower amount of mobile Snf1 would lead to a higher degree of phosphorylation in the available Snf1 and an increase in nucleocytoplasmic shuttling. Whereas under low glucose conditions tested in our experiment, Snf1, besides the possibility of halt in translation, could serve other functions than glucose signaling or is part of a stationary complex in the nucleus. This would fit with a model where nucleocytoplasmic shuttling is regulated by the Snf1 phosphorylation status and its interaction with Gal83 as response to the type and concentration of carbon source that determines its localization to the nucleus.

Further, we show that upon addition of fermentable sugars in various concentrations to cells grown in ethanol, Mig1 nuclear localization inversely correlates with the phosphorylation status of Snf1, linking inactivation of Snf1 with spatial distribution of one of its target proteins, which is in agreement with data reporting that Mig1 nuclear localization depends on Snf1-dependent phosphorylation [26].

Snf1-dephosphorylation was observed for 0.005% glucose, mannose, and fructose, with a more distinctive dephosphorylation for glucose. We report Mig1 localizing to the nucleus at 0.005% glucose, in accordance with previously reported results [30, 42]. Our results contribute to that, in so far as we observed Mig1 nuclear localization at concentrations of 0.05% and above for mannose and fructose. For all hexoses, the Mig1 nuclear intensity increased in a dose-dependent manner, however, the trend of increase over concentration seems to be hexose specific.

The above observations could be a consequence of differing import rates of the tested hexose sugars, as for example the maximum import rate of glucose is lower than the import rate of fructose [43]. Alternatively, it could be the result of differing first steps of metabolism for the tested sugars, since only glucose is rapidly converted to glucose-6-phosphate, which was shown to stimulate Snf1 dephosphorylation [44]. It has furthermore been suggested that hexokinases which take part in the regulation of Mig1 in connection with Snf1 might exert their regulative function in a manner dependent on the type of hexose in the medium [31].

It remains unclear whether the above processes, a combination, or other regulatory mechanisms impact Mig1 phosphorylation by Snf1 and/or dephosphorylation by Reg1/Glc7.

HXK1 and *SUC2* are subject to glucose repression mediated by Mig1. Our results indicate that glucose de-repression mediated by Snf1 could start already at concentrations of 0.05% glucose, where Mig1 is located mostly in the cytosol. Snf1 activity is necessary to mediate glucose de-repression, but interestingly Snf1 is showing a decreased phosphorylation ratio at 0.005% glucose and increased nucleocytoplasmic shuttling, strengthening the argument that Snf1 is more readily dephosphorylated in the presence of glucose, while Mig1 localizes to the nucleus as response to concentration of glucose. Previous studies revealed both a Snf1-dependent as well as -independent dephosphorylation of Mig1 [33] and considering the fluctuations in environmental changes and the necessity of the cell to adapt to these, it seems plausible that mechanisms other than change in transcription through Mig1

might be at play [37].

Cellular signaling pathways are essential to sense and respond to external stimuli such as nutrients and other environmental cues, as well as their dynamic changes. At the systems level, a complex network of kinases and phosphatases plays a major role in the regulation of signaling pathways which are involved in the control of metabolism, cell cycle and growth [45–48] .

The data presented in this paper reinforce the notion that not only the activation/inactivation of kinases but also their subcellular localization and that of their targets influence fate decisions in response to environmental changes.

Materials and Methods

Strain maintenance and growth conditions

If not stated otherwise, yeast strains were grown at 30°C in synthetic complete medium, containing 1.7 g/l yeast nitrogen base, 5 g/l ammonium sulfate, 670 mg/l complete supplement mix here referred to as YNB with appropriate drop out where applicable; supplemented with carbon source as indicated by the specific experiments. All media components except for carbon source were obtained from Formedium.

Strains used in this study are listed in Table 2.

To ensure functionality of Snf1-GFP constructs, we conducted a spot test on non-feasible carbon sources that would lead to a decrease in growth if Snf1 functionality is impaired (see Figure S3).

Fluorescence Recovery After Photobleaching (FRAP)

Strain BY4741 SNF1-GFP was grown in YNB supplemented with 2% glucose to exponential phase, OD/ml ≈ 0.3, and immobilized on an 8-well chambered coverglass (Ibidi) coated with poly-L-lysine (Sigma). Media were switched to YNB with either 2% glucose, 0.05% glucose or 2% glycerol and incubated at 30°C for 1 h before imaging to ensure adaptation to the new carbon source. At least 21 cells distributed over three separate experiments per condition were imaged on a LSM700 laser scanning confocal microscope (Zeiss) using a Plan-Apochromat 63x /1.4 oil immersion objective, pinhole set to 1 AU for the longest wavelength and kept constant over all channels. FRAP was performed on GFP-tagged Snf1, excitation 488 nm, emission 518 nm, 2x zoom with framesize 596x596, pixel size of 0.09μm and pixel dwell time of 0.9 μs. The cells were continuously imaged for 100 frames, and bleaching was done in 100 bursts at 100% at 488 nm after 5 pre-scans using a circular ROI covering the nucleus. To determine fluorescence decay by acquisition, a reference area of adjacent cells was captured, as well as a circular ROI for baseline determination. Determination of bleach area covering the nucleus was achieved by imaging the nuclear marker mCherry-tagged Nrd1 (excitation: 555 nm, emission: 572 nm) and drawing a circular ROI around the determined area.

For image processing, the average fluorescence intensity as well as diameter of the imaged areas was extracted from the time-lapse image series for each image using the software ZEN2012 Black (Zeiss). Given the values for background intensity, the intensity for the nuclear region, as well as a reference region containing adjacent cells in the same frame, the measured intensities were processed by first removing background signal and normalizing prebleach phase to 1 by calculating the ratio of measured intensity at a given timepoint over the mean of intensities measured in the frames pre-bleach for both, the reference and the bleached region. Measurements that were aberrating due to cell movement were removed from the dataset after visual inspection of the acquired time series. Correction for acquisition bleaching was done in RStudio, version 1.4.1106 [49], by calculating the median of the normalized reference regions and fitting the curve according to the following equation:

$$I_{ref}(t) = I_{0ref} A_{ref} e^{\tau_{ref} * t}$$

With $I_{0ref} = 0$ representing the baseline as fluorophores become bleached completely and data have been corrected for background noise.

With the parameters A_{ref} and τ_{ref} estimated by nonlinear least squares regression, measured FRAP intensities were interpolated and further used for nonlinear mixed effect modeling.

Data available at: 10.6084/m9.figshare.25397809 (FRAP movies) and 10.6084/m9.figshare.25397803 (FRAP Raw data).

Non-linear mixed effect model

Non-linear mixed-effects modelling is typically used for longitudinal data exhibiting both within- and in-between-subject variability [50]. This method has been widely used in pharmacokinetic and pharmacodynamic studies [51, 52], but in recent years it is utilized in single-cell time-lapse data and facilitating our understanding of cell-to-cell variability [32, 36, 53–55]. When analyzing fluorescence measurements of a tagged protein in single cells over time, the observed intensity will differ between measurements even if the cells are in a steady-state, due to measurement error. Moreover, owing to extrinsic variability, imaged fluorophores within cells will display different intensity levels. Using a mixed-effects framework, the observed cell-to-cell variability can be accounted for in the analysis by letting the rate parameters vary between cells according to a probability distribution. Furthermore, a mixed-effects framework allows the assessment of potential correlations between parameters in different cells.

To analyze dynamic measurements for Snf1-GFP from the FRAP experiment, a non-linear mixed-effect regression was implemented and simulated in Monolix (version 2023R1) [56, 57]. The data, project files and models are available at the following github repository: https://github.com/cvijoviclab/Snf1-localization .

Assuming reaction dominant recovery, FRAP curves were fitted to a single exponential equation, summarizing experiments across conditions tested:

$$I = I_0 + A * \left(1 - e^{-\tau * t}\right)$$

I_0 represents the degree of bleaching, *A* is the mobility constant, τ is the kinetic constant of bound/unbound species and *t* is the time after bleach.

Speed of recovery can be calculated by determining the recovery half max time where 50% of the plateau of estimated fluorescence recovery is reached:

$$\tau_{1/2} = \frac{ln0.5}{-\tau}$$

TABLE 2 ● Strains used in this study.

Name	Relevant genotype
BY4741	*MATa his3Δ1 leu2Δ0 met15Δ0 ura3Δ 0*
BY4741 SNF1-GFP	*MATa his3Δ1 leu2Δ0 met15Δ0 ura3Δ 0 SNF1-GFP-HIS3MX NRD1-mCherry-Hph*
W303-1A	*MATa leu2-3,112 trp1-1 can1-100 ura3-1 ade2-1 his3-11,15*
W303-1A MIG1-GFP	*MATa leu2-3,112 trp1-1 can1-100 ura3-1 ade2-1 his3-11,15 NRD1mCherry-Hph MIG1-GFP-KanMX*
W303-1A snf1Δ	*MATa leu2-3,112 trp1-1 can1-100 ura3-1 ade2-1 his3-11,15 snf1::KanMX*

Mobile and immobile phase according to this model are represented as:

$$Mobile\ phase = A - I_0$$

$$Immobile\ phase = 1 - (A - I_0)$$

Steady-state localization microscopy

Strain BY4741 SNF1-GFP was grown in YNB supplemented with 2% glucose to exponential phase and immobilized on an 8-well chambered coverglass (Ibidi) coated with poly-L-lysine (Sigma). Media were exchanged by centrifugation and resuspended in YNB with either 2% glucose, 0.05% glucose or 2% glycerol at least 1 h before imaging to ensure adaptation to the new carbon source. At least 20 cells/condition were imaged on either ELYRA PS.1 SIM/PAL-M LSM780 (Zeiss) using Plan-Apochromat 40x /1.4 oil immersion objective.

Cell segmentation, extraction of mean intensities and background removal was done in the ImageJ distribution of Fiji [58] and MATLAB _R2019b. Plots and statistical analysis were done using RStudio, version 1.4.1106 [49].

As the dataset did not pass the Shapiro–Wilk test, a non-parametric equivalent of ANOVA was used, the Kruskal-Wallis test. For pairwise comparison, a Wilcox test with Bonferroni correction was performed. These statistical tests were done in RStudio, version 1.4.1106 [49] .

Short-timescale microfluidic experiments

Strain W303-1A was transformed with MIG1-GFP-KanMX and NRD1-mCherry hphNT1 using standard methods for yeast genetics and transformation [59]. Cells were grown to mid-exponential phase in YNB supplied with 3% ethanol overnight. A glass-bottom petri dish (GWST-5030, WillCo Wells, UK) was treated with concanavalin A solution (1 mg/ml in 10 mM Tris-HCl buffer, 100 mM NaCl, adjusted to pH 8.0 using 5 M HCl) for 30 min at room temperature. The concanavalin A solution was removed and incubated for 5 min at 30°C after the cell suspension was added. Cells which did not adhere to the surface were removed by washing with YNB containing 3% ethanol. Exposure of cells to different conditions was performed using a BioPen system (Fluicell AB, Sweden) and an environmental chamber to hold the temperature at 30°C during exposure. Experiments were performed on an inverted microscope Olympus cellR widefield microscope system, based on an inverted IX81 motorized microscope with a Xe light source (MT20) and a Hamamatsu C8484 CCD camera. Images were acquired using a U PlanS Apo 40x NA 0.95l objective. The filter cubes, light intensities and exposure time and light intensities for all imaging channels used were as following for GFP: excitation 472/30 nm, emission 520/35 nm with an intensity of 20% for 350 ms. mCherry: excitation 560/40 nm, emission 630/75 nm with an intensity of 20% for 150 ms. The microscope and the microfluidic device were controlled using the Experiment Manager in the Xcellence software. Three images with an axial distance of 0.8 μm were acquired in transmission and fluorescent channels. The acquisition time for one set of images at each time point was ≈15 s. Images were acquired at changing imaging intervals to reduce phototoxicity and bleaching while keeping appropriate timing to monitor changes in Mig1 localization. Time-lapse imaging was performed three times every 30 s until the media shift, followed by 15 times every 20 s, followed by five times every 120 s, adding up to an overall experiment time of 16 min. Brightfield images acquired above the focal plane were divided by images acquired below the focal plane using custom Matlab Scripts. Division of images leads to the elimination of uneven illumination and enhances the diffraction pattern of cells. Segmentation was performed on the resulting images using CellX [60]. The Mig1-localization index was calculated from the CellX output as follows:

$$Localization\ index\ = \frac{Median\ fluorescence\ nucleus}{Median\ fluorescencecell} - 1$$

Cells were tracked using custom MATLAB scripts according to previously described methods [61].

Western Blot analysis of Snf1 phosphorylation

Cell lysates were prepared as described in Caligaris *et al.* [62]. After denaturation at 98°C for 5 min, samples subjected to SDS-PAGE and transferred onto nitrocellulose membranes. After 1 h blocking with blocking buffer (5% milk powder in tris-buffered saline), membranes were immunoblotted with anti-pT172-AMPK (Cell Signaling, 1:1000 dilution) or anti-Cdc34 (1:5000 dilution) primary antibodies [63]. After three washes, the membranes were incubated with anti-rabbit secondary antibodies conjugated to horseradish peroxidase, washed again three times, and developed with ECL (GE Healthcare).

Bands were quantified using the Image lab software (Bio-Rad) and quantification results were plotted as phosphorylation ratio relative to the control condition containing ethanol, normalized to Cdc34.

RNA extraction and qPCR

Cells were collected by filtration and rapidly frozen at -80°C. RNA extraction and qPCR were performed as in Tripodi *et al.* [40]. Briefly, cells were resuspended in LETS buffer (200 mM LiCl, 20 mM EDTA, 20 mM Tris-HCl, SDS 20%), phenol:chloroform:isoamyl alcohol (PCI) was added and cells were lysed by vortex-mixing with glass beads. A second step of PCI separation was performed. RNA was selectively precipitated

with LiCl (0.5 M) at -80°C. 40 μg of RNA was treated with 6 units of DNase I (Jena Biosciences) for 1 h at 37°C, followed by PCI extraction and ethanol precipitation at -80°C. Reverse transcription of 0.5 μg mRNA was carried out with iScript cDNA Synthesis Kit (BIO-RAD). Quantitative Real-time PCR for SUC2 and HXK1 gene expression was performed by using ChamQ Universal SYBR pPCR Master Mix (Vazyme) on a CFX Connect Real-Time PCR System (BIO-RAD). The obtained data were normalized on CDC28 and CDC34 reference genes and the sample before the upshift was set to 1; data were analyzed with Maestro CFX software (BIO-RAD).

Acknowledgments

This work was supported by the Swedish Research Council (VR2016-03744, VR2017-05117 and VR2023-04319) and the Swedish Foundation for Strategic Research (FFL15-0238) to MC and the grant 2023-ATE-0068 to F.T. (Fondo di Ateneo Quota Dipartimentale, FAQD, Università degli Studi di Milano-Bicocca). We acknowledge the Centre for Cellular Imaging at the University of Gothenburg and the National Microscopy Infrastructure, NMI (VR-RFI 2019-00217) for providing assistance in confocal microscopy and FRAP.

Conflict of interest

None declared.

SUPPLEMENTAL MATERIAL

All supplemental data for this article are available online at www.microbialcell.com.

Please cite this article as: Svenja Braam, Farida Tripodi, Linnea Österberg, Sebastian Persson, Niek Welkenhuysen, Paola Coccetti, Marija Cvijovic (2024). Exploring carbon source related localization and phosphorylation in the Snf1/Mig1 network using population and single cell-based approaches . Microbial Cell 11: 143-154. doi: 10.15698/mic2024.05.822

REFERENCES

1. Hardie DG, Ross FA, Hawley SA (2012). AMP-Activated Protein Kinase: A Target for Drugs both Ancient and Modern. Chem Biol 19 (10): 1222–1236. doi:10.1016/j.chembiol.2012.08.019

2. Hardie D (2014). AMPK-Sensing Energy while Talking to Other Signaling Pathways. Cell Metab 20 (6): 939–952. doi:10.1016/j.cmet.2014.09.013

3. Abate G, Bastonini E, Braun KA, Verdone L, Young ET, Caserta M (2012). Snf1/AMPK regulates Gcn5 occupancy, H3 acetylation and chromatin remodelling at S. cerevisiae ADY2 promoter. Biochim Biophy Acta 1819 (5): 419–427. doi:10.1016/j.bbagrm.2012.01.009

4. Coccetti P, Nicastro R, Tripodi F (2018). Conventional and emerging roles of the energy sensor Snf1/AMPK in Saccharomyces cerevisiae. Microbial Cell 5 (11): 482–494. doi:10.15698/mic2018.11.655

5. Hedbacker K (2008). SNF1/AMPK pathways in yeast. Front Biosci 13 (13): 2408. doi:10.2741/2854

6. Zhang J, Olsson L, Nielsen J (2010). The β-subunits of the Snf1 kinase in Saccharomyces cerevisiae, Gal83 and Sip2, but not Sip1, are redundant in glucose derepression and regulation of sterol biosynthesis: Snf1 kinase in glucose derepression. Mol Microbiol 77 (2): 371–383. doi:10.1111/j.1365-2958.2010.07209.x

7. Usaite R, Jewett MC, Oliveira AP, Yates JR, Olsson L, Nielsen J (2009). Reconstruction of the yeast Snf1 kinase regulatory network reveals its role as a global energy regulator. Mol Syst Biol 5 (1): 319–319. doi:10.1038/msb.2009.67

8. Hong SP, Carlson M (2007). Regulation of Snf1 Protein Kinase in Response to Environmental Stress⁎. J Biol Chem 282 (23): 16,838–16,845. doi:10.1074/jbc.M700146200

9. Jiang R, Carlson M (1997). The Snf1 protein kinase and its activating subunit, Snf4, interact with distinct domains of the Sip1/Sip2/Gal83 component in the kinase complex. Mol Cell Biol 17 (4): 2099–2106. doi:10.1128/MCB.17.4.2099

10. Schmidt MC (2000). beta-subunits of Snf1 kinase are required for kinase function and substrate definition. EMBO J 19 (18): 4936–4943. doi:10.1093/emboj/19.18.4936

11. Vincent O, Townley R, Kuchin S, Carlson M (2001). Subcellular localization of the Snf1 kinase is regulated by specific β subunits and a novel glucose signaling mechanism. Genes Dev 15 (9): 1104–1114. doi:10.1101/gad.879301

12. Celenza JL, Eng FJ, Carlson M (1989). Molecular analysis of the SNF4 gene of Saccharomyces cerevisiae: evidence for physical association of the SNF4 protein with the SNF1 protein kinase. Mol Cell Biol 9 (11): 5045–5054. doi:10.1128/MCB.9.11.5045

13. Chandrashekarappa DG, Mccartney RR, Donnell AFO, Schmidt MC (2016). The β subunit of yeast AMP-activated protein kinase directs substrate specificity in response to alkaline stress. Cell Signal 28 (12): 1881–1893. doi:10.1016/j.cellsig.2016.08.016

14. Garcia-Salcedo R, Lubitz T, Beltran G, Elbing K, Tian Y, Frey S, Wolkenhauer O, Krantz M, Klipp E, Hohmann S (2014). Glucose de-repression by yeast AMP-activated protein kinase SNF1 is controlled via at least two independent steps. FEBS J 281 (7): 1901–1917. doi:10.1111/febs.12753

15. Hong SP, Leiper FC, Woods A, Carling D, Carlson M (2003). Activation of yeast Snf1 and mammalian AMP-activated protein kinase by upstream kinases. Proc Nati Acad Sci U S A 100 (15): 8839–8843. doi:10.1073/pnas.1533136100

16. Nath N, Mccartney RR, Schmidt MC (2003). Yeast Pak1 Kinase Associates with and Activates Snf1. Mol Cell Biol 23 (11): 3909–3917. doi:10.1128/MCB.23.11.3909-3917.2003

17. Gancedo JM (1998). Yeast Carbon Catabolite Repression. Microbiol Mol Biol Rev 62 (2): 334–361. doi:10.1128/MMBR.62.2.334-361.1998.

18. Ruiz A, Xu X, Carlson M (2013). Ptc1 Protein Phosphatase 2C Contributes to Glucose Regulation of SNF1/AMP-activated Protein Kinase (AMPK) in Saccharomyces cerevisiae. J Biol Chem 288 (43): 31,052–31,058. doi:10.1074/jbc.M113.503763

19. Ruiz A, Xu X, Carlson M (2011). Roles of two protein phosphatases, Reg1-Glc7 and Sit4, and glycogen synthesis in regulation of SNF1 protein kinase. Proc Nat Acad Sci U S A 108 (16): 6349–6354. doi:10.1073/pnas.1102758108

20. Zhang Y, Mccartney RR, Chandrashekarappa DG, Mangat S, Schmidt MC (2011). Reg1 Protein Regulates Phosphorylation of All Three Snf1 Isoforms but Preferentially Associates with the Gal83 Isoform. Eukaryot Cell 10 (12): 1628–1636. doi:10.1128/EC.05176-11

21. Frederick DL, Tatchell K (**1996**). The REG2 Gene of Saccharomyces cerevisiae Encodes a Type 1 Protein Phosphatase-Binding Protein That Functions with Reg1p and the Snf1 Protein Kinase to Regulate Growth. **Mol Cell Biol** 16 (6): 2922–2931. doi:10.1128/MCB.16.6.2922

22. Ostling J, Ronne H (**1998**). Negative control of the Mig1p repressor by Snf1p-dependent phosphorylation in the absence of glucose. **Eur J Biochem** 252 (1): 162–168. doi:10.1046/j.1432-1327.1998.2520162.x

23. Treitel MA, Kuchin S, Carlson M (**1998**). Snf1 Protein Kinase Regulates Phosphorylation of the Mig1 Repressor in Saccharomyces cerevisiae. **Mol Cell Biol** 18 (11): 6273–6280. doi:10.1128/MCB.18.11.6273

24. Treitel MA, Carlson M (**1995**). Repression by SSN6-TUP1 is directed by MIG1, a repressor/activator protein. **Proc Nati Acad Sci U S A** 92 (8): 3132–3136. doi:10.1073/pnas.92.8.3132

25. Keleher CA, Redd MJ, Schultz J, Carlson M, Johnson AD (**1992**). Ssn6-Tup1 is a general repressor of transcription in yeast. **Cell** 68 (4): 90,146–90,150. doi:10.1016/0092-8674(92)90146-4

26. Devit MJ, Johnston M (**1999**). The nuclear exportin Msn5 is required for nuclear export of the Mig1 glucose repressor of Saccharomyces cerevisiae. **Curr Biol** 9 (21): 1231–1241. doi:10.1016/S0960-9822(99)80503-X

27. Carlson M, Osmond BC, Botstein D (**1981**). Mutants of yeast defective in sucrose utilization. **Genetics** 98 (1). doi:10.1093/genetics/98.1.25

28. Lutfiyya LL, Iyer VR, Derisi J, Devit MJ, Brown PO, Johnston M (**1998**). Characterization of Three Related Glucose Repressors and Genes They Regulate in Saccharomyces cerevisiae. **Genetics** 150 (4): 1377–1391. doi:10.1093/genetics/150.4.1377

29. Lutfiyya LL, Johnston M (**1996**). Two zinc-finger-containing repressors are responsible for glucose repression of SUC2 expression. **Mol Cell Biol** 16 (9): 4790–4797. doi:10.1128/MCB.16.9.4790

30. Bendrioua L, Smedh M, Almquist J, Cvijovic M, Jirstrand M, Goksor M, Adiels CB, Hohmann S (**2014**). Yeast AMP-activated protein kinase monitors glucose concentration changes and absolute glucose levels. **J Biol Chem** 289 (18): 12,863–12,875. doi:10.1074/jbc.M114.547976

31. Schmidt GW, Welkenhuysen N, Ye T, Cvijovic M, Hohmann S (**2020**). Mig1 localization exhibits biphasic behavior which is controlled by both metabolic and regulatory roles of the sugar kinases. **Mol Genetics Genom** 295 (6): 1489–1500. doi:10.1007/s00438-020-01715-4

32. Welkenhuysen N, Borgqvist J, Backman M, Bendrioua L, Goksör M, Adiels CB, Cvijovic M, Hohmann S (**2017**). Single-cell study links metabolism with nutrient signaling and reveals sources of variability. **BMC Syst Biol** 11 (1): 59–59. doi:10.1186/s12918-017-0435-z

33. Wollman AJ, Shashkova S, Hedlund EG, Friemann R, Hohmann S, Leake MC (**2017**). Transcription factor clusters regulate genes in eukaryotic cells. **Elife** 6. doi:10.7554/eLife.27451

34. Ye T, Elbing K, Hohmann S (**2008**). The pathway by which the yeast protein kinase Snf1p controls acquisition of sodium tolerance is different from that mediating glucose regulation. **Microbiol** 154 (9): 2814–2826. doi:10.1099/mic.0.2008/020149-0

35. Vega M, Riera A, Fernández-Cid A, Herrero P, Moreno F (**2016**). Hexokinase 2 Is an Intracellular Glucose Sensor of Yeast Cells That Maintains the Structure and Activity of Mig1 Protein Repressor Complex. **J Biol Chem** 291 (14): 7267–7285. doi:10.1074/jbc.M115.711408

36. Karlsson M, Janzén DLI, Durrieu L, Colman-Lerner A, Kjellsson MC, Cedersund G (**2015**). Nonlinear mixed-effects modelling for single cell estimation: when, why, and how to use it. **BMC Syst Biol** 9 (1): 1–15. doi:10.1186/s12918-015-0203-x

37. Tripodi F, Nicastro R, Reghellin V, Coccetti P (**2015**). Post-translational modifications on yeast carbon metabolism: Regulatory mechanisms beyond transcriptional control. **Biochim Biophys Acta** 1850 (4): 620–627. doi:10.1016/j.bbagen.2014.12.010

38. Özcan S, Johnston M (**1995**). Three Different Regulatory Mechanisms Enable Yeast Hexose Transporter (HXT) Genes To Be Induced by Different Levels of Glucose. **Mol Cell Biol** 15 (3): 1564–1572. doi:10.1128/MCB.15.3.1564

39. Yin Z, Hatton L, Brown AJP (**2000**). Differential post-transcriptional regulation of yeast mRNAs in response to high and low glucose concentrations. **Mol Microbiol** 35 (3): 553–565. doi:10.1046/j.1365-2958.2000.01723.x

40. Tripodi F, Nicastro R, Busnelli S, Cirulli C, Maffioli E, Tedeschi G, Alberghina L, Coccetti P (**2013**). Protein Kinase CK2 Holoenzyme Promotes Start-Specific Transcription in Saccharomyces cerevisiae. . **Eukaryot Cell** 12 (9): 1271–80. doi:10.1128/ec.00117-13

41. Hsu HE, Liu TN, Yeh CS, Chang TH, Lo YC, Kao CF (**2015**). Feedback Control of Snf1 Protein and Its Phosphorylation Is Necessary for Adaptation to Environmental Stress. **J Biol Chem** 290 (27): 16,786–16,796. doi:10.1074/jbc.M115.639443

42. Devit MJ, Waddle JA, Johnston M (**1997**). Regulated nuclear translocation of the Mig1 glucose repressor. **Mol Biol Cell** 8 (8): 1603–1618. doi:10.1091/mbc.8.8.1603

43. Berthels NJ, Otero RRC, Bauer FF, Pretorius IS, Thevelein JM (**2008**). Correlation between glucose/fructose discrepancy and hexokinase kinetic properties in different Saccharomyces cerevisiae wine yeast strains. **Appl Microbiol Biotechnol** 77 (5): 1083–1091. doi:10.1007/s00253-007-1231-2

44. Milanesi R, Tripodi F, Vertemara J, Tisi R, Coccetti P (**2021**). AMPK Phosphorylation Is Controlled by Glucose Transport Rate in a PKA-Independent Manner. **Int J Mol Sci** 22 (17): 9483. doi:10.3390/ijms22179483

45. Alberghina L, Coccetti P (**2009**). Systems biology of the cell cycle of Saccharomyces cerevisiae: From network mining to system-level properties. **Biotechnol Adv** 27 (6): 960–978. doi:10.1016/j.biotechadv.2009.05.021

46. Milanesi R, Coccetti P, Tripodi F (**2020**). The Regulatory Role of Key Metabolites in the Control of Cell Signaling. **Biomolecules** 10 (6): 862. doi:10.3390/biom10060862

47. Tripodi F, Zinzalla V, Vanoni M, Alberghina L, Coccetti P (**2007**). In CK2 inactivated cells the cyclin dependent kinase inhibitor Sic1 is involved in cell-cycle arrest before the onset of S phase. **Biochem Biophys Res Commun** 359 (4): 921–7. doi:10.1016/j.bbrc.2007.05.195

48. Shashkova S, Welkenhuysen N, Hohmann S (**2015**). Molecular communication: crosstalk between the Snf1 and other signaling pathways. **FEMS Yeast Res** 15 (4): fov026. doi:10.1093/femsyr/fov026

49. Team R (**2020**). RStudio: Integrated Development Environment for R. RStudio

50. Davidian M, Giltinan DM (**2003**). Nonlinear models for repeated measurement data: An overview and update. **JABES** 8 (4): 387–419. doi:10.1198/1085711032697

51. Lavielle M, Mentré F (**2007**). Estimation of Population Pharmacokinetic Parameters of Saquinavir in HIV Patients with the MONOLIX Software. **J Pharmacokinet Pharmacodyn** 34 (2): 229–249. doi:10.1007/s10928-006-9043-z

52. Sissoko D, Laouenan C, Folkesson E, M'Lebing AB, Beavogui AH, Baize S, Camara AM, Maes P, Shepherd S, Danel C, Carazo S, Conde MN, Gala JL, Colin G, Savini H, Bore JA, Marcis FL, Koundouno FR, Petitjean F, Lamah MC, Diederich S, Tounkara A, Poelart G, Berbain E, Dindart JM, Duraffour S, Lefevre A, Leno T, Peyrouset O, Irenge L (**2016**). Experimental Treatment with Favipiravir for Ebola Virus Disease (the JIKI Trial): A Historically Controlled, Single-Arm Proof-of-Concept Trial in Guinea. **PLOS Med** 13 (3): 1001,967–1001,967. doi:10.1371/journal.pmed.1001967

53. Almquist J, Bendrioua L, Adiels CB, Goksör M, Hohmann S, Jirstrand M (**2015**). A Nonlinear Mixed Effects Approach for Modeling the Cell-To-Cell Variability of Mig1 Dynamics in Yeast. **PLOS ONE** 10 (4): e124,050–124,050. doi:10.1371/journal.pone.0124050

54. Llamosi A, Gonzalez-Vargas AM, Versari C, Cinquemani E, Ferrari-Trecate G, Hersen P, Batt G (**2016**). What Population Reveals about Individual Cell Identity: Single-Cell Parameter Estimation of Models of Gene Expression in Yeast. **PLOS Comput Biol** 12 (2): e1004,706. doi:10.1371/journal.pcbi.1004706

55. Persson S, Welkenhuysen N, Shashkova S, Wiqvist S, Reith P, Schmidt GW, Picchini U, Cvijovic M (**2022**). Scalable and flexible inference framework for stochastic dynamic single-cell models. **PLOS Comput Biol** 18 (5): e1010,082. doi:10.1371/journal.pcbi.1010082

56. Kuhn E, Lavielle M (**2005**). Maximum likelihood estimation in nonlinear mixed effects models. **Computational Statistics & Data Analysis** 49 (4): 1020–1038. doi:10.1016/j.csda.2004.07.002

57. (**2023R1 M**). Lixoft SAS, a Simulations Plus company

58. Schindelin J, Arganda-Carreras I, Frise E, Kaynig V, Longair M, Pietzsch T, Preibisch S, Rueden C, Saalfeld S, Schmid B, Tinevez JY, White DJ, Hartenstein V, Eliceiri K, Tomancak P, Cardona A (**2012**). Fiji: An open-source platform for biological-image analysis. **Nat Met** 9 (7): 676–682. doi:10.1038/nmeth.2019

59. Gietz RD, Woods RA (**2002**). Transformation of yeast by lithium acetate/single-stranded carrier DNA/polyethylene glycol method. **Methods Enzymol** 350: 87–96. doi:10.1016/s0076-6879(02)50957-5

60. Mayer C, Dimopoulos S, Rudolf F, Stelling J (**2013**). Using CellX to Quantify Intracellular Events. **Curr Protoc Mol Biol** 101 (1). doi:10.1002/0471142727.mb1422s101

61. Ricicova M, Hamidi M, Quiring A, Niemistö A, Emberly E, Hansen CL (**2013**). Dissecting genealogy and cell cycle as sources of cell-to-cell variability in MAPK signaling using high-throughput lineage tracking. **Proc Nati Acad Sci U S A** 110 (28): 11,403–11,408. doi:10.1073/pnas.1215850110

62. Caligaris M, Nicastro R, Hu Z, Tripodi F, Hummel JE, Pillet B, Deprez MA, Winderickx J, Rospert S, Coccetti P, Dengjel J, De Virgilio C (**2023**). Snf1/AMPK fine-tunes TORC1 signaling in response to glucose starvation. **Elife** 12: e84,319. doi:10.7554/eLife.84319

63. Coccetti P, Tripodi F, Tedeschi G, Nonnis S, Marin O, Fantinato S, Cirulli C, Vanoni M, Alberghina L (**2008**). The CK2 phosphorylation of catalytic domain of Cdc34 modulates its activity at the G1 to S transition in Saccharomyces cerevisiae. **Cell Cycle** 7 (10): 1391–1401. doi:10.4161/cc.7.10.5825